Resourcesat-1 Data Quality Evaluation System

S.S. Palsule, Bankim Shah, G. Paswan, Anuja Sharma,
Anjali Garg, Hetal Pandya,
Shailendra S. Srivastava, Sampa Roy

Data Quality Evaluation Division, RESIPA,
Space Application Center, ISRO,
Ahmedabad 15, India

30 April 2007

Abstract
In continuation of IRS-1C/1D mission, Resourcesat mission was planned for integrated land and water resource management. Resourcesat was launched on 17 October 2003. This satellite carries three multi-spectral cameras with variable swath and different spatial resolution. Data quality evaluation (DQE) system characterizes payload and platform performance and its impact on radiometric and geometric accuracies achieved on user product during initial and operational phase. DQE system is software system where each parameter package is integrated in DQE scheduler, which automates and facilitates the execution procedure.

Table of Contents

1. INTRODUCTION

Resourcesat-1 satellite was launched on 17 October 2003, from Sriharikota (India) by PSLV launch vehicle. Resourcesat-1 satellite has mainly three payloads: a multi-spectral LISS-3 camera having medium spatial resolution (23.5 m) with four bands (three VNIR, one SWIR), an advanced wide field sensor with two heads mounted as AWiFS-A and AWiFS-B camera having coarser spatial resolution 56 m (at Nadir) with same four bands (three VNIR, one SWIR) and a high spatial resolution 5.8 m (at Nadir) multi-spectral LISS-4 camera with only VNIR band. The objective of the mission is to support various types of data products generation on operational basis for integrated land and water resource management. This objective is achieved by characterizing sensor and platform performance and its impact on radiometric and geometric accuracies achieved on user product during initial phase. Subsequently Resourcesat data quality evaluation (DQE) system monitors these accuracies and compare with specification during operational phase of mission. The process of characterization and monitoring is performed by data quality evaluation system. This system is conceptualized as per mission specific requirement and Hardware/Software System configuration planned at operational agency National Remote Sensing Agency (NRSA). The system design, development and implementation phase is carried out at Data Quality Evaluation Division, SAC, Ahmedabad and operationalized at DQE work centre NRSA, Balanagar, Hyderabad (Internal Technical Document, 2001). The various activities performed for this system is given in Fig. 1.

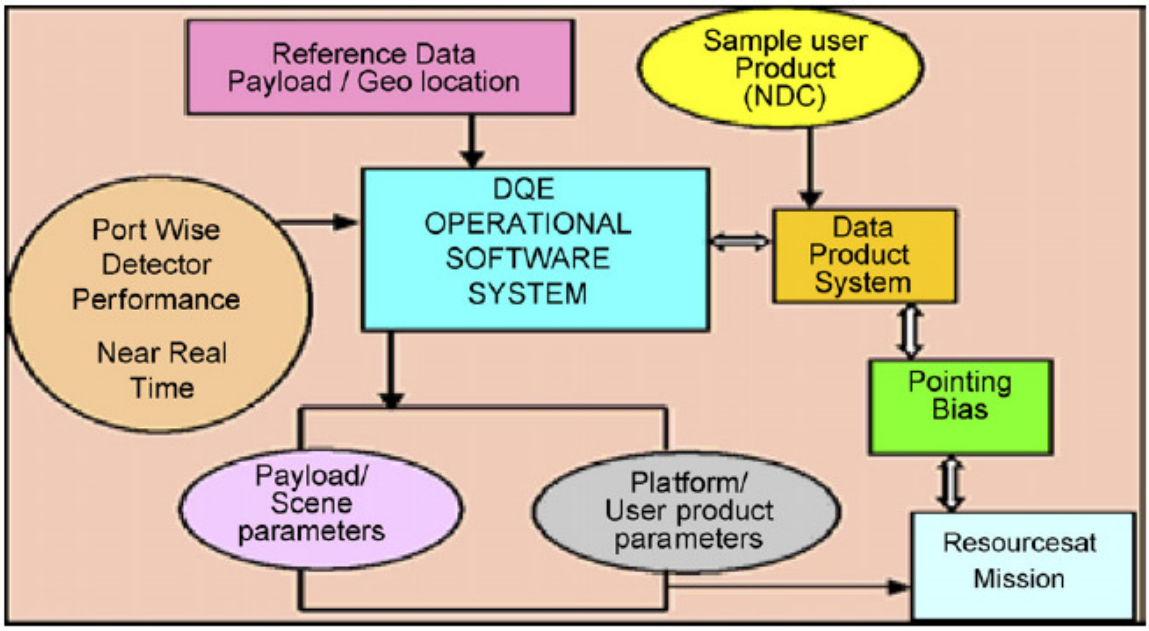

Fig. 1. DQE activity flow diagram. NDC: National Data Center, NRSA, Hyderabad.

The activity flow diagram emphasis on reference data generation prior to launch from laboratory measured data for sensor performance evaluation and geodetic reference generation for products geo-location analysis. The data quality evaluation system is primarily software system where sample user product from data product work centre are routed to DQE work centre for performance evaluation (Dube et al., 1998).

The objective of this paper is to demonstrate the statistical results achieved for onboard sensors performance and product accuracies to qualify Resourcesat mission products.

2. DQE PARAMETERS

The various system specific DQE parameters have been considered for Resourcesat mission. The user product specific operational DQE parameters are being monitored routinely at NRSA for all missions. These parameters are classified to evaluate payload performance, platform sensor performance and its impact on radiometric and geometric qualities of user products (Maeda et al., 1987). DQE system analyzes in-flight onboard calibration data with CALDQE package. The payload specification and user product specification given in Tables 1 and 2 are studied for DQE system parameter formulation (Internal Technical Document, 2002).

Payload specifications

S. no.	Parameters	LISS-3	LISS-4	AWiFS	
1	Spatial resolution (m)	23.5	5.8 (at Nadir)	56 (at Nadir)	
2	Swath (km)	141	23.9 (MX), 70.3 (MONO)	740 with two heads	
3	Spectral bands	Bands 2, 3, 4, 5	Bands 2, 3, 4	Bands 2, 3, 4, 5	
4	Quantization bits				
	Generated	7[a], 10[b]	10	10	
	Transmitted	7[a], 7[b]	7	10	
5	SNR @ Sat. radiance	>128	>128	>512	
6	Saturation radiance[c]			A	B
	B2	12.06 G3	27.16 G2	59.81	52.34
	B3	15.13 G3	23.05 G2	45.81	40.75
	B4	15.75 G3	17.20 G2	32.42	28.42
	B5	03.41 G2	36.77	06.94	04.64
7	BBR (pixel)	±0.25	±0.25	±0.25	
8	Operating temperature	20 ± 2 °C For B5: 23.5 °C, 25 °C	20 ± 2 °C For B5: 23.5 °C, 25 °C	20 ± 2 °C For B5: 23.5 °C, 25 °C	
9	SWR @ Nyq.				
	B2	>0.40	>0.20	>0.30	
	B3	>0.40	>0.20	>0.30	
	B4	>0.35	>0.20	>0.20	
	B5	>0.20	>0.20	>0.20	

Off Nadir viewing capability for LISS-4: ±26°.
[a] VNIR.
[b] SWIR.
[c] $mW/cm^2/sr/\mu m$.

Table 1 – Payload Specifications

Data products specifications

S. no.	Product type	Level of correction	Sensor
1	Path–row based (with and without shift)	(a) Raw (b) Radiometrically corrected (c) Standard (d) Geo-referenced	LISS-3 AWiFS-A and B
2	Scene based	(a) Raw (b) Radiometrically corrected (c) Standard (d) Geo-referenced	LISS-4
3	Map sheet based	(a) Geocoded (15′ × 15′) (b) Geocoded (7.5′ × 7.5′) (c) Geocoded (1° × 1°)	LISS-3, LISS-4 LISS-4 AWiFS-A and AWiFS-B
4	Floating quadrant	(a) Standard (b) Geo-referenced	LISS-3
5	Point based	Geocoded (5′ × 5′)	LISS-4
6	Basic stereo pair	Radiometrically corrected	LISS-4

Table 2 – Data Product Specifications

Following parameters are visualized for system analysis and feed back to Resourcesat mission.

2.1. Payload related

- Detector port performance by way of histogram analysis (odd, even, all detectors) of few scan lines at regular interval for all four sensors.

- Detector performance evaluation using in-flight calibration data. (In-flight calibration reference data is generated at satellite integrated thermovac testing.)

- Band-to-band registration (on radiometric corrected product for LISS-3 and AWiFS, on corrected product in case of LISS-4).

2.2. Platform related

- Estimation of scene based residual roll, pitch and yaw bias (pointing bias) using GCPs and reference images.

2.3. Scene based radiometric parameters

- Histogram of full scene, odd/even detector histogram and computation of corresponding scene dynamic range, at sensor target radiance comparison at given Sun latitude position.

- Relative radiometric behavior of pseudo-invariant ground features with respect to saturation radiance.

2.4. User product geometric parameters

- Location accuracy, scale, internal distortion (local variations/standard deviation of feature distances). The evaluation and analysis procedure supports all mission defined level of products in super structure and Geo-tiff format.

2.5. Payload related

2.5.1. Detector port histogram analysis

The push broom imaging concept is implemented using a linear CCD placed in the focal plane of optics.

The four spectral bands are realized using independent and separate refractive optical assemblies for each band. Detectors for VNIR bands are 6000 element devices with a pixel size of 10 mm and 7 mm on a pixel pitch of 10 mm with two video output ports is used. Detector for SWIR band is also 6000 elements staggered array device with a pixel size of 13 mm _ 13 mm on a pixel pitch of 13 mm and line pitch of 26 mm with two video output ports is used. These two video ports form continuous image in both direction. The partial failure of CCD devices or port will result as reductions in scene resolution/swath/FCC quality for user data utilization. The scene data in remote sensing application is primarily characterized by scene histogram. A scene histogram is representation of the occurrence of gray count recorded by a sensor as seen and reflected from the terrain. This simple definition implies that occurrence denotes the continuous frequency of each reflected intensity recorded by every detector element at given instant. During payload pass data acquisition a set of 1000 lines at some interval are selected for detector port histogram generation. These histogram files are analyzed by PORT HIST package with following rules for quantifying detector port performance. The basic ideology of the package is that the histogram generated by the even and odd ports of the detector array must be nearly same.

Sample histogram plot for few scan lines of two ports (LISS-3 camera) indicates that successive pixel gray count is within five counts (Fig. 2.1). Overall port count difference is within expected values (_20 counts) for data acquired simultaneously from all four cameras.

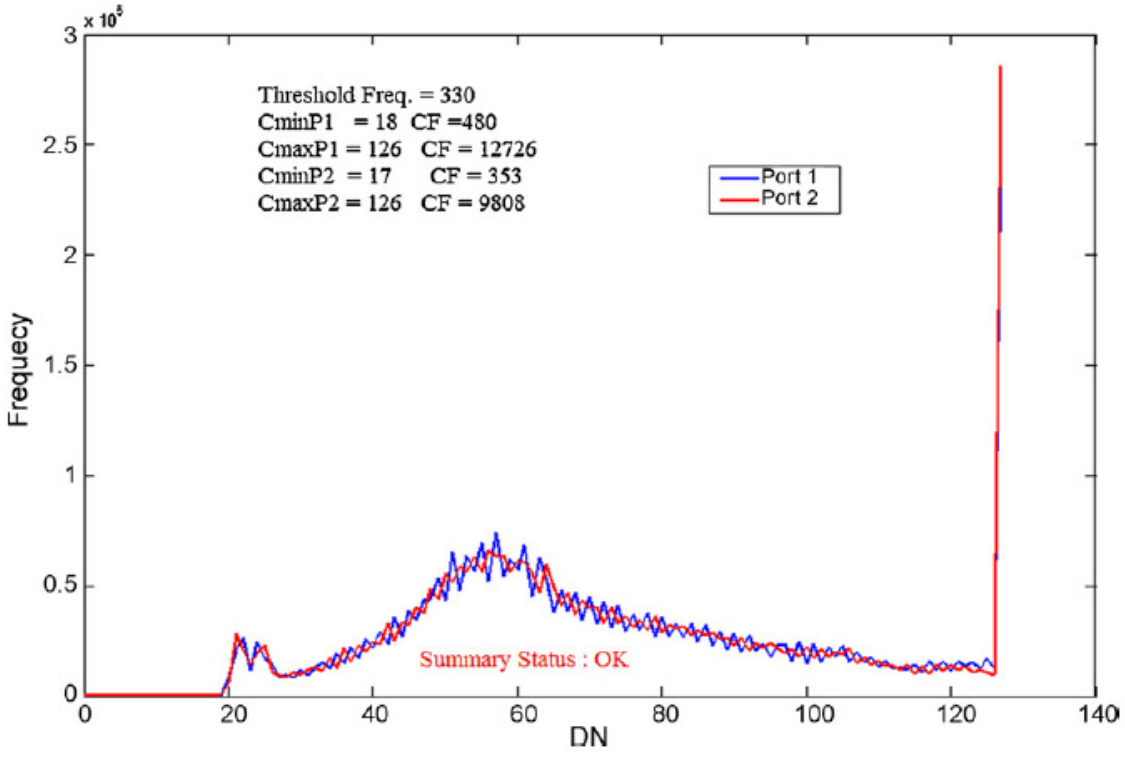

Fig. 2.1. Resourcesat-1, LISS-3, 06 November 2003, Band 2, Histogram P1 and P2.

Rule 1—Indication of port failure: The histogram files for different ports are verified whether the frequency for any count is equal to the sum of all the frequencies in the port, if ‘‘Yes’’ then flash a message ‘‘Frequency for all counts is zero’’, which suggests port failure.

Rule 2—Indication of trend of port behavior: If frequency for minimum and maximum counts does not exist (which means that the frequency for the Zero Count is not equal to the total number of detectors in the port then flash a message ‘‘Frequency for all the counts is very low’’ (less than limit frequency value).

Rule 3—Flagging of inter-port identical behavior: If the histogram files for different ports are identical then flash a message ‘‘Histograms for different ports are identical’’ suggesting artificial trend.

Rule 4—Flagging of inter-port behavior: In the event of getting frequency and magnitude of minimum and maximum counts, the following conditions are checked and appropriate message flashed.

The magnitude and frequency of minimum count for even and odd port of given line will have similar numbers.

A. If difference of magnitude of minimum count for two ports is greater than the expected threshold value measured from the calibration data, flash a message ‘‘Difference in the magnitude of minimum count for the ports is high’’.

B. If difference of corresponding frequencies of minimum count of two ports is greater than 10% of sum of the frequencies in the histogram, flash a message ‘‘Difference of frequencies indicating normal/abnormal behavior of the port’’. Both of these conditions are applied to the magnitude and frequency of maximum count of even and odd port of given set of lines and appropriate message flashed.

Both of these conditions are applied to the magnitude and frequency of maximum count of even and odd port of given set of lines and appropriate message flashed. Another point worth mentioning here is that conditions are applied for the main peak of the histogram after rejecting the noisy data for the analysis. The port performance of all four cameras is consistent over a period of 3 years.

2.5.2. In-flight calibration data analysis

The provision of in-flight calibration of CCDs using LEDs exists for VNIR and SWIR bands (Internal Technical Document, 2002). Four LEDs per detector array for both VNIR and SWIR bands are being used. The type of LEDs for VNIR is HPIN6092 and for SWIR it is C86072E. There are basically two schemes for in-flight calibration namely exposure based and CAL pulse mode. In exposure based scheme, LEDs are continuously illuminated and exposure width is varied for obtaining fixed 16 calibration levels. The optical schematic of illumination with LEDs position is shown in Fig. 2.2.

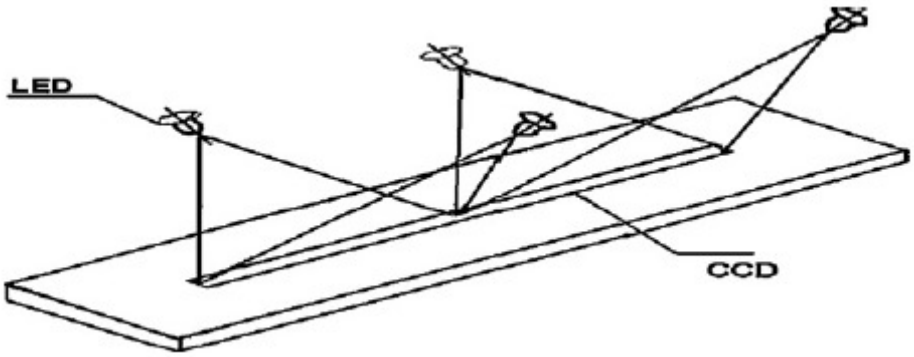

Fig. 2.2. LED configurations

A set of 16 lines consists of all 16 exposure levels and such 100 sets of lines are used for computing statistical parameter of individual detector performance.

In CAL pulse based calibration scheme the LEDs are illuminated with different pulse width. The full calibration cycle consist of 2048 lines of the data in which one illumination line is followed by seven dark lines. In first half of the calibration cycle (1024 lines) intensities I1 (LED1 50% on, LED2 off), I2 (LED1 50% off, LED2 50% on), I3 (LED1 50% on, LED2 50% on) and in the second half of the cycle intensities I4 (LED1 100% on, LED2 off), I5 (LED1 off, LED2 100% on) and I6 (LED1 100% on, LED2 100% on) are repeated alternately after seven dark current lines.

Exposure based scheme is adopted for AWiFS-A, AWiFS-B and LISS-4 camera for VNIR band and CAL pulse based scheme is adopted for LISS-3 VNIR, SWIR and AWiFS SWIR bands.

Parameters. The statistical parameters for each detector, port and array levels are computed for dark current and various intensity levels generated by two different in-flight calibration schemes. The parameters are:

- Intensity mean count and standard deviation for (a) each detector, (b) detectors of even and odd ports, (c) detectors of detector array level.
- Difference of intensity mean count for (a) even and odd ports, (b) ground measured and in-flight measured detector mean (standard error), (c) successive two data set of in-flight measured data for detectors (relative error).
- Flagged detector based on Chi-square fit.

This in-flight calibration data of each sensor is available prior to launch in various thermovac condition and same data set is monitored after launch periodically. The mean, standard deviation, even and odd port difference are plotted for each detector to characterize detector performance. The detail analysis and characterization is performed for each band using in-house developed CALDQE package. The in-flight calibration data is acquired by scheduling CAL MODE for payload data acquisition. This analysis monitors detector performance with laboratory measured sensor performance and any deviation or failure of detector is alarmed as flagged detector.

The criteria applied for detector flagging is based on Chi-square goodness of fit statistics. Chi-square fit is statistical representation which measures the goodness of fit of observations, representing the close agreement between the current observed values and reference values, it really measures the trend of current observation and compares with trend of previous ground reference observations taken in similar environment.

The basic hypothesis of Chi-square fit is that the gray value obtained onboard at given time for each intensity will follow the same distribution as that of the gray values obtained on ground.

A small deviation for all intensity levels within threshold will have similar trend of normal detector performance, while deviation above the threshold limit for all intensity levels reflects either degradation or failure. A sample plot of flagged detector for AWiFS-A SWIR band is given in Fig. 2.3.

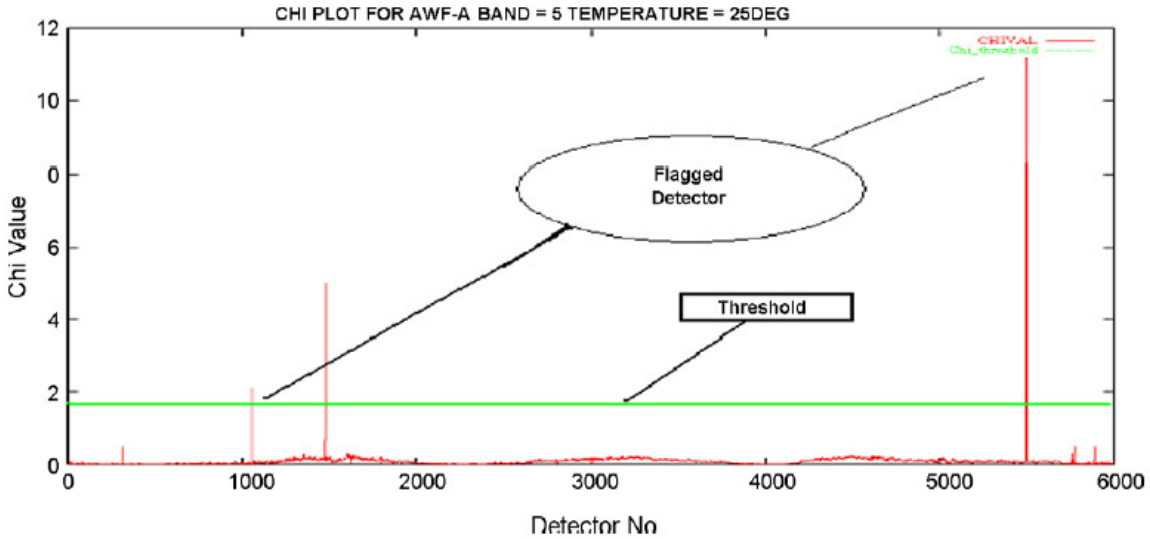

Fig. 2.3. AWiFS-A band: 5 flagged detector.

The in-flight intensity data patterns of detector array for all VNIR bands of all four cameras are consistently matching within five counts over a period of 3 years. This behavior indicates the good performance of VNIR detectors and trend of detector degradation/failure is seen for SWIR band.

2.5.3. Band-to-band registration

In multi-spectral imaging, the pixel-to-pixel registration between any two bands is defined as the area of overlap between the images viewed by the corresponding detector elements (Brown, 1992). Band-to-band registration is important parameter of user product, which quantifies the accuracy of per pixel area classification. This parameter at payload performance level is a function of (a) matching of image format of lens assemblies, (b) active length of detector array for each band, (c) matching of individual band distortion among all bands, (d) ability to register the band physically. This

parameter is measured in laboratory by single line acquisition method where special target is kept at the focal plane of a collimator and illuminated by uniform light source. The target is imaged simultaneously by all bands and shift in centroid position for each band is measure of misregistration. This registration parameter stability is a function of change in format of telescope and stability of detector head assembly in the mechanical mount.

This parameter is monitored by in-house developed BBR package.

The algorithms for the computations of band-to-band misregistration for user product evaluation are: (a) Sequential Similarity Detection Algorithm (SSDA) and (b) Mean Bias Correlation based Algorithm.

The package computes the across track and along track translation registration among the different band images at pixel level (Inglade and Giros, 2004). The registration process is carried out in following four steps: (a) selection of features in each image, (b) reference generation, (c) computation and (d) estimation of misregistration value.
Feature selection: Relative control points (RCPs) are manually identified. RCPs are the points, which can be uniquely identified in all band images as cross roads, railway crossings, sharp edges, tip of rivers (bends), etc.

Reference generation: One band image is considered as reference image and all other band images are compared with this reference image. Search area of M _ M pixels is being extracted from reference image and window area of N _ N pixel is selected from the other image (where M > N).

Computation: Window area is moved in search area for the all-possible combinations. Error value is computed using Eq. (1) for SSDA method and Mean Bias for Correlation coefficient is computed by correlation method using Eq. (2).

Sequential Similarity Detection Algorithm:

Error matrix value (*i, j*)

$$= \sum_i \sum_j [(\mathrm{gw}_{ij} - \mathrm{mw}) - (\mathrm{gs}_{ij} - \mathrm{ms})] \qquad (1)$$

where gw is the gray value of window image at (i, j), gs is the gray value of the search image at (i, j), ms is the mean value of search area, mw is the mean value of window area, i and j varies from 1 to N (N _ N is the size of window area).

Mean Bias Correlation Method:

Correlation coefficient (*i, j*)

$$= \frac{\sum_i \sum_j [(\mathrm{gw}_{ij} - \mathrm{mw})(\mathrm{gs}_{ij} - \mathrm{ms})]}{\mathrm{sqrt}(\sum_j \mathrm{gw}_{ij} - \mathrm{mw})^2 \sum_j (\mathrm{gs}_{ij} - \mathrm{ms}))} \qquad (2)$$

where gw is the gray value of window image at (i, j), gs is the gray value of the search image at (i, j), ms is the mean value of search area, mw is the mean value of window area, i and j varies from 1 to N (N _ N is the size of window area).

Estimation of misregistration value: The best pixel matching point in two band images is given by minimum error value position in SSDA method, while highest value of correlation coefficient between two band images gives the best registration in Mean Bias Correlation Method. The pixel matching or registration is at integer pixel level, which is further processed at sub-pixel level by surface fitting of second order/fourth order polynomial.

During laboratory measurement exercise a profile at every 300 pixel interval was generated for SWIR band of LISS-3 and AWiFS cameras. The SWIR band had unsymmetrical distribution of registration with VNIR band and scale factor correction was required for format mismatch for both cameras. Scene based statistical profile was generated by DQE system by evaluating various terrain product and it was corrected by Data Product system during geometric resampling process. However this misregistration was further refined to register SWIR band with VNIR band within 0.3 pixels for both cameras.

In case of LISS-4 sensor, the VNIR bands are separated in along track direction by 14.5 km, the additional platform attitude information is applied for band registration before resampling process. The VNIR registration of LISS-4 camera is within 0.6 pixels for 90% of the scenes generated and evaluated.

2.5.4. Sidelap/overlap between two heads of AWiFS

AWiFS camera with two heads make a swath of 740 km, the individual heads in along track direction makes sub-scene as (AWiFS-A, AWiFS-C) and (AWiFS-B, AWiFS-D). The same individual heads in across direction make sub-scene (AWiFS-A, AWiFS-B) and (AWiFS-C, AWiFS-D). The common area between two sub-scenes in across direction is termed as Sidelap which varies with latitude.

The common area between two sub-scenes in along direction is termed as overlap of scene, which is a function of time, used for scene framing. The estimated Sidelap between two heads is shown in Table 3, which has constant value at different latitude. The scan line variation in Sidelap area depicts the geo-location variation of two sub-scenes, which is adjusted and corrected in Data Product system. The Sidelap area of two heads is used for mosaicing the scene and providing radiometric balance between two sub-scenes. The estimated overlap area between two sub-scenes of AWiFS in Table 4 depicts the adjustment of scene framing time for correct representation of geo-location area.

Sensor	Results	Latitude (°)
AWFA and AWFB	138.67 pixel, scan diff: 22	25.8
AWFA and AWFB	138.57 pixel, scan diff: 18	15.56
AWFA and AWFB	138.50 pixel, scan diff: 17	7.58

Table 3 - Sidelap (common area between AWFA and AWFB at different latitude)

	Results	Specifications
AWFA and AWFC	196.6 scan lines, 11.01 km	150 scan lines
LISS-3	304.8 scan lines, 7.3 km	321 scan lines

Table 4 - Overlap (common area between two successive scenes)

2.6. Platform related

The pointing bias is a gross representation of known camera and platform sensor misalignment angle along with imaging attitude information. This knowledge is accounted in Data Product system for standard product generation. The uncertainty of attitude measured values from platform sensors (star sensor, gyro sensor) during imaging, deviation of camera alignment angle after launch, seasonal variation gives platform residual pointing bias which results as geo-location error on standard product. It is possible to characterize payload and attitude sensor geometry on ground with precise known ground control points. The initial phase evaluation exercise on test bed quantifies the residual magnitude of mounting angle. Subsequently the platform performance variation is monitored daily from three scene per pass and accumulated biases over a period of 3 months is examined. This dynamic phenomenon occurs from seasonal variation an onboard fixed frame axis variation which is finally accounted as constant lump values in data processing chain for improving user product accuracies. This phenomenon is visualized as uncertainty error in roll/pitch/yaw direction w.r.t. Nadir height. This parameter is computed as displacement of image point coordinates and corresponding map coordinates in along and across direction. The pictorial representation of displacement is given in Fig. 2.4 and displacement of coordinates due to roll, pitch, yaw effect is given in Eqs. (3)–(6).

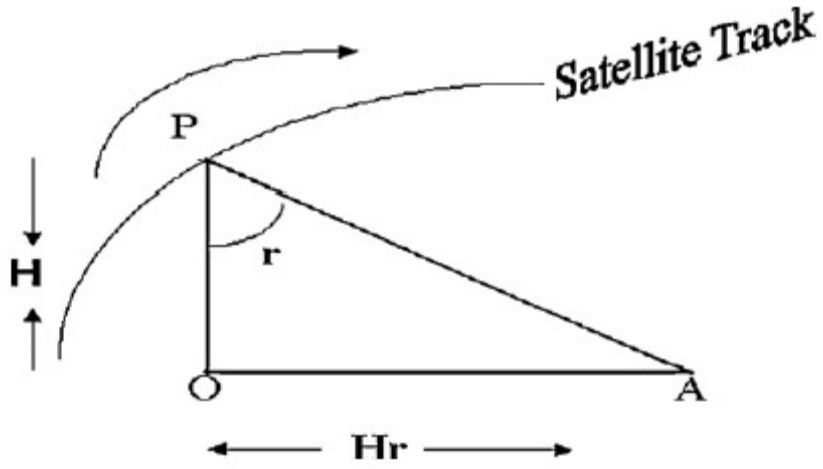

Fig. 2.4. Displaced image coordinates.

$$X_i^1 = X_i + Hr \,(\text{roll effect}) \tag{3}$$

$$Y_i^1 = Y_i - H\,p \,(\text{pitch effect}) \tag{4}$$

where H is the altitude, $X_i,\ Y_i,\ X_i^1,\ Y_i^1$ are image coordinates in image and ground plane and r and p are the residual roll and pitch.

$$\begin{bmatrix} X_m \\ Y_m \end{bmatrix} = \begin{bmatrix} \cos(\gamma) & 0 \\ \sin(\gamma) & 1 \end{bmatrix} \begin{bmatrix} X_i^1 \\ Y_i^1 \end{bmatrix} (\text{yaw effect}) \tag{5}$$

Combined equation of residual attitude is

$$\begin{bmatrix} X_m \\ Y_m \end{bmatrix} = \begin{bmatrix} \cos(\gamma) & 0 \\ \sin(\gamma) & 1 \end{bmatrix} \begin{bmatrix} X_i + Hr \\ Y_i + H\,p \end{bmatrix} \tag{6}$$

$(X_m, Y_m), (X_i, Y_i)$ are the map and image coordinates, g is the residual yaw. The values of r, p and g computed by using weighted least square technique (Ford and Zanelli, 1985). During initial phase the magnitude of pointing bias for roll and pitch direction was 0.08° and 0.1 °, respectively. Simultaneously the values are tuned of the order 0.001 ° in all three directions.

2.7. Scene based radiometric parameters

The push broom imaging technique uses the detector array width and the focal length of optics in across track direction for scene swath, and the detector array advances a distance equal to one resolution element and new scan line is generated. The number of scan lines with scene swath for four bands generates scene false color composite. The signal strength reaching from target is a measure of radiometric performance of sensor. Radiance reaching at sensor level is a sensor response function, which is a combined effect of weighted integrated effect of spectral and spatial response (Richter et al., 1998). A linear relationship between sampled and quantized digital number and signal energy falling at sensor exists. This relation is established by illuminating total camera system with white light source as reference and measuring digital number as camera output for input radiance reaching from white light source. The pseudo-invariant features like Rajasthan desert sand, Barren land, lake water of same geoposition are monitored for mean signal count as target energy falling on detector (Dinguirard and Slatter, 1999). The variation of detector count is a measure of feature variability and system noise contribution due to photon, quantization and electron uncertainty. The signal to noise ratio is a measurement of noise present for signal mean intensity recorded by detector. At sensor radiance is a converted value of signal mean count using system response function. Same feature have been monitored for all previous missions. The ground measured feature radiance value for all bands is compared with at sensor radiance for quantifying relative radiance response of all cameras. Apparent reflectance is normalized target radiance value for Sun position (Berger and Kaufmanns, 1995).

Dynamic range of system is the recording capability of minimum and maximum target energy reaching at sensor. This is computed by scene histogram. The AWiFS sensor radiance setting cover target features from water to snow and clouds in all bands. The different stages of snow are clearly visible. The dynamic range of AWiFS is 53 mW/cm2/sr/l. The LISS-4 sensor radiance setting also cover 100% Albedo for VNIR band with 10-bit quantization but only 7-bits are transmitted. The selection of combination of number of bits gives four gain setting, which increases or decreases the dynamic range of sensor (Desai and Palsule, 2002). All these parameters are computed by in-house developed RDQE package. A typical radiometric analysis of given target for LISS-3 and AWiFS sensor is given in Tables 5a and 5b.

S. no.	Band	Mean count	S.D.	SNR	Rad[3]	%App Reflect
1	2	145.50	1.73	84.00	7.93	20.04
2	3	123.20	1.58	77.95	8.11	23.55
3	4	101.12	0.97	104.15	6.96	29.46
4	5	127.58	1.15	110.78	1.75	33.62

Sun elevation: 41.8; DOP: 28 October 2003; place: Iran; target: desert sand; Rad[3]: $mW/cm^2/sr/\mu m$.

Table 5a - Relative radiance behavior for LISS-3

S. no.	Band	Mean count	S.D.	SNR	Rad[3]	%App Reflect
1	2	134.37	2.08	64.57	6.88	17.90
2	3	163.11	2.41	67.43	6.50	19.43
3	4	191.12	2.69	70.82	5.31	23.15
4	5	327.00	3.44	94.90	2.17	42.98

Sun elevation: 40.3; DOP: 28 October 2003; place: Iran; target: desert sand; Rad[3]: $mW/cm^2/sr/\mu m$.

Table 5b - Relative radiance behavior for AWiFS

The relative radiance of standard target for LISS-3 and AWiFS sensor is given in Figs. 2.5 and 2.6. The inter-sensor radiance for VNIR bands are within 5% and SWIR band is within 15% as expected. (Due to imaging geometry and filter response characteristics of individual cameras.)

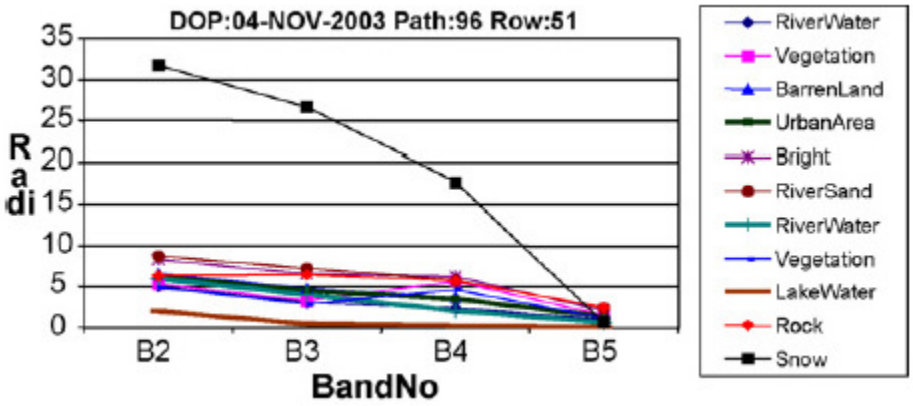

Fig. 2.5. Relative radiance of standard target for AWiFS.

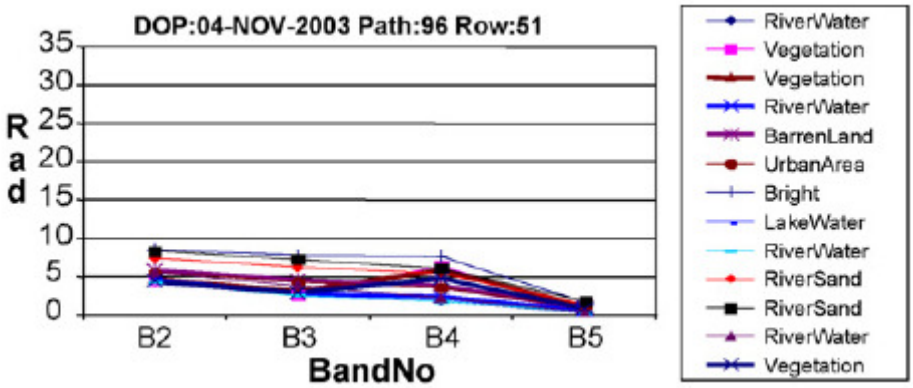

Fig. 2.6. Relative radiance of standard target for LISS-3.

2.8. User product geometric parameters

The best estimate of orbit and attitude information is used by Data Product system for generating image grid or tick mark information for assigning geo-location value of each pixel image data (Ganas and Athanassios, 2000). The deviation of assigned geo-location value of pixel w.r.t. actual precise measured GCP's results in geo-location error. The image viewed by different sensor should have same geo-location value on final corrected standard product. The geometric accuracy of standard product is a measure of image grid registration with map grid of same area in a suitable scale. These parameters are visualized as:

Geo-location accuracy: The root mean square (RMS) error of all differences of ground control points coordinates observed on product with image grid and map is known as location accuracy of product.

Scale: The mean of ratio of distance on map and image is defined as scale of a digital product.

The variations in location error on plain terrain (minimum terrain height variation of selected scenes and reference scene is within 15 m) with respect to selected reference

points are known as internal distortion of a product. The analysis of variation in location error has improved the understanding and application of onboard attitude sensor measured values for improving product accuracies.

The user product image geodetic grid with video information is displayed on screen and corresponding reference area is also viewed for comparison and evaluation. The process of comparing requires transformation in two planes as briefed here.

Image to ground mapping (forward coefficient generation)

$$X = a_0 + a_1 x + a_2 y$$

$$Y = b_0 + b_1 x + b_2 y$$

where (x, y) is scan line, pixel number and (X, Y) are respective northing, easting of a GCP converted using map projection equation (Snyder, 1983). The six parameters a_0, a_1, a_2, b_0, b_1, b_2 are the forward transformation coefficient. The pair (a_0, b_0) denotes the translation of origin. The rotation angle, affinity angle and scale in both directions is derived from remaining four coefficients (a_1, a_2, b_1, and b_2).

The forward transformation can be written in matrix form as:

$$\begin{bmatrix} X \\ Y \end{bmatrix} = \begin{bmatrix} a_0 \\ b_0 \end{bmatrix} + \begin{bmatrix} a_1 & a_2 \\ b_1 & b_2 \end{bmatrix} \begin{bmatrix} x \\ y \end{bmatrix} \tag{7}$$

Ground to image mapping (backward coefficient generation) the inverse of this transformation exists which is as follows

$$\begin{bmatrix} x \\ y \end{bmatrix} = \begin{bmatrix} a_1 & a_2 \\ b_1 & b_2 \end{bmatrix} \begin{bmatrix} X - a_0 \\ Y - b_0 \end{bmatrix} \tag{8}$$

This can be further simplified as

$$x = a_{11}(X - a_0) + a_{21}(Y - b_0)$$

$$y = b_{11}(X - a_0) + b_{21}(Y - b_0)$$

is the backward transformation equation.

The six parameters a_0, b_0, a_{11}, a_{21}, b_{11}, b_{21} are the backward transformation coefficient. The four parameters a_{11}, a_{21}, b_{11}, b_{21} are the element of inverse of rotation matrix.

These transformations are solved using precise GCPs. The deviation of image and reference information is computed all over scene for statistical trend representation

(Kardoulas et al., 1996). The same combination of image and reference points are used for computing, the scale of product and assessing the local variations within product as internal distortion. The user product geometric accuracy is monitored by in-house developed GDQE package. The sample result for each sensor product is given in Appendix A.

3. REFERENCE IMAGE LIBRARY

The Resourcesat mission operations requirements were that gross level platform pointing and user product bias could be estimated with LISS-3 reference image of coarser accuracy (50 m) (Zhou and Li, 2000). The use of reference image database gives operational ease and flexibility for product evaluation, which is independent of path/row scheme, swath, and spatial resolution of data, quantization and season. Every scan pixel of image has geo-location accuracy within 50 m which means scene evaluation is possible based on identifiable feature specific points as compare to ground or map measured ground control points. IRS-1D LISS-3 reference images over Indian landmass were generated using 1:50,000 scale maps by designer team in collaboration with Regional Remote Sensing Service Centre (RRSSC), Nagpur. These 220 reference images are stored in ORACLE database. This database contains metadata and image file name. Image files are maintained separately. Based on user products corner coordinates, reference images are retrieved from database where each scan/pixel of image can be associated with geo-location value within 50-m accuracy.

The availability of LISS-3 reference images over Indian landmass and navigation facility for GCP identification has increased through put rate for product evaluation. A summary of products evaluated for each sensor in a period of 35 days is given in Table 6.
The accuracy of reference images was validated independently and number of scenes with associated geo-location accuracy is given in Fig. 2.7.

S. no.	Sensor	No. of products
1	LISS-3	120
2	AWiFS	294
3	L4 MONO	27
4	L4 MX	128

Table 6 - Sensor wise products evaluated

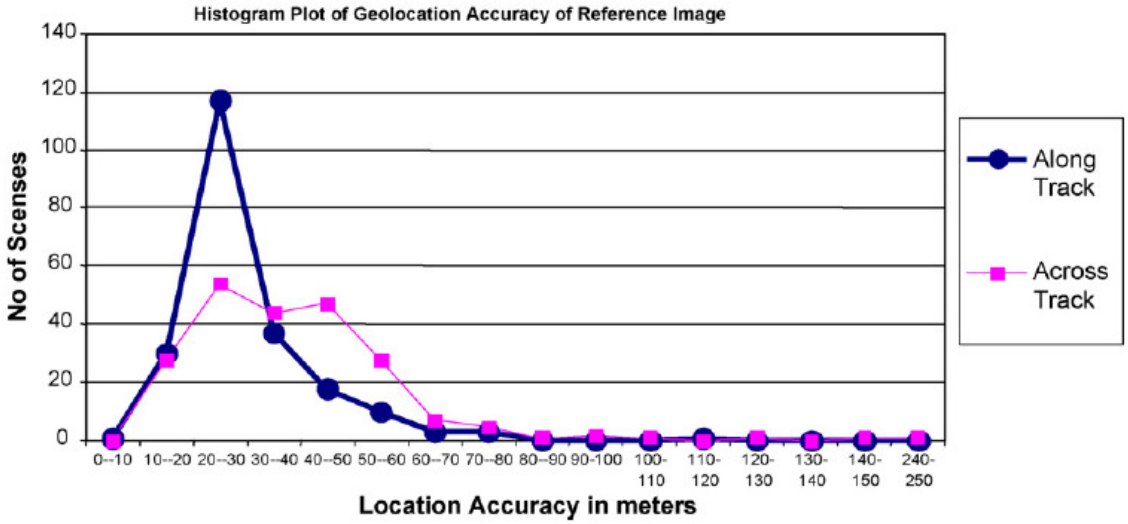

Fig. 2.7. Accuracy representations of reference images.

4. CONCLUSIONS

Data quality evaluation system is software system where each category of parameter is defined, algorithm is developed and process are packaged as PORTHIST ANAL, RDQE, CALDQE, BBR, REFGEN, GDQE, and DATABASE. All these packages are integrated in DQE scheduler which facilitates and automates the software process execution from Data Ingest, Display, Computation to store parameter results in respective database. Routine daily reports are generated for circulation and feedback to mission. The Resourcesat product performance is as follow:

4.1 Geometric quality

Geometric quality of LISS-3 data products (for 100% cases)
- Location accuracy _300 m (100%)
- Internal distortion 3 pixel RMSE
- Scale change 0.5%
- BBR 0.25 pixel for B2, B3, B4, B5

AWiFS data products (for 100% cases of AWiFS-A and 90% cases of AWiFS-B)
- Location accuracy _300 m
- Internal distortion 2 pixel RMSE
- Scale change 0.1%
- BBR 0.3 pixel for B2, B3, B4, B5

LISS-4 MX data products (for 90% cases)
- Location accuracy _300 m
- Internal distortion 10 pixel RMSE
- Scale change 0.05%
- BBR 0.6 pixel for B2, B3, B4

4.2 Radiometric quality

LISS-3 sensor

Quantization level 127 count

Dynamic range at gain 1 ($mW/cm^2/sr/\lambda$)

B2	26.0
B3	27.0
B4	20.69
B5	6.9

Relative band behavior for VNIR1.1%

SNR $\leq$127

AWiFS sensor

Quantization level 1023 count

Dynamic range at exposure 8

B2	52.3(E8)
B3	40.7(E9)
B4	28.4(E8)
B5	4.6

Relative band behavior for VNIR1.8%

SNR $\leq$512

LISS-4 sensor

Quantization level 1023 count

Transmitted 127 count

Dynamic range at MS2 (gain)

B2	27.16
B3	23.0
B4	17.23

Relative band behavior for VNIR_1.2%

SNR $\leq$127

APPENDIX A - SAMPLE RESULTS OF USER PRODUCT GEOMETRIC PARAMETERS

Scene info.	Geo-location (m)		Scale (m)	DQE computed residual attitude (°)
Sensor, orbit tilt angle (°)	RMS Lat., Lon.	Mean/S.D. Lat./Lon., Lat./Lon.	Scale, S.D., %variation	Roll, pitch, yaw
DOP: 16 July 2004, Prod type: ST path/row: 96/51				
AWFC, 3880	327.59, 123.46	−321.88/97.96, 60.93/75.130	56.000, 1.36, 0.001	0.006716, 0.022288, 0.007152
AWFC, 3880	302.91, 175.65	−264.73/138.16, 147.22/108.460	56.017, 0.095, 0.030	0.009608, 0.018300, 0.008778
L-3, 3880	248.91, 37.96, 0.00	−247.59/−3.78, 25.63/37.770	23.994, 0.021, 0.026	−0.000947, 0.016981, 0.014768
DOP: 16 July 2004, Prod type: ST path/row: 102/60				
L-4, 3880, −2.11	447.56, 143.33	−445.12/−142.27, 46.68/17.400	5.008, 0.015, 0.146	−0.009820, 0.030729, 0.318503

REFERENCES

Berger, M., Kaufmanns, H., 1995. Mom S-02-D2/STS-55, Mission Validation of Spectral and Panchromatic Modules. GIS 2/1995, PP21-30.

Brown, L.G., 1992. A survey of image registration techniques, ACM. Computing Surveys 24 (4), 325–376.

Desai, Y.P., Palsule, S.S., 2002. In-flight characterization of TES-PAN sensor on Chharodi Test Site. ISPRS TC-VII December 2002.

Dinguirard, M., Slatter, P.N., 1999. Calibration of space multi spectral imaging sensor, a review. Remote Sensing and Environment 68.

Dube, N., et al., 1998. Integrated software for IRS Data Products System. In: Proceedings of ISPRS (International Society of Photogrammetry & Remote Sensing) symposium, February 1998, Bangalore.

Ford, G.E., Zanelli, C.I., 1985. Analysis and quantification of errors in the geometric correction of satellite images. Photogrammetric Engineering and Remote Sensing 51 (November (11)), 1725– 1734.

Ganas, A., Athanassios, E., 2000. A comparative study on the production of satellite ortho imagery from geological remote sensing. Geocarto International 15 (June (2)).

Inglade, J., Giros, A., 2004. On the possibility of automatic multisensor image registration. IEEE Transaction on Geo-science & Remote Sensing 42 (October (10)), 2004. Internal Technical Document of Remote Sensing Application and Image Processing Area, SAC, ISRO, Ahmedabad. IRS-P6/DQE/SAC/RESIPA/DQED/April-2001.

Internal Technical Documents Published by Sensor Development Area, SAC, ISRO, Ahmedabad. EOSG/OMG/SAC/SEDA/Feb-2002.

Kardoulas, N.G., Bird, A.C., Lawan, A.I., 1996. Geometric correction of Spot and Landsat imagery. A comparison of map and GPS derived control points. Photogrammetric Engineering and Remote Sensing 62 (October (10)), 1173–1177.

Maeda, K., et al., 1987. Some results of a MOS-1 airborne verification experiment—multispectral electronic self-scanning radiometric (MESSR). IEEE Transactions on Geosciences and Remote Sensing GE-25 (November (6)), 788–795, doi:10.1109/TGRS.1987.289750.

Richter, R., Beisl, U., Muller, A., 1998, In-flight calibration of IRS-1C in Europe, DLR-1B 552-07/98.

Snyder, J.P., 1983. Map Projection used by US Geological Survey.

Zhou, G., Li, R., 2000. Accuracy evaluation of ground control points from IKONOS high-resolution satellite imagery. Photogrammetric Engineering & Remote Sensing 66 (September (9)), 1103–1112.